Steady flow past non-uniform wire grids

By J. H. McCARTHY

Hydromechanics Laboratory, David Taylor Model Basin, Washington

(Received 15 September 1963 and in revised form 10 February 1964)

A solution is obtained for steady, moderately sheared, three-dimensional flow past a wire grid of arbitrary resistance distribution which is placed normal to the axis of a duct of arbitrary but constant cross-section. The formulation presented is an extension of those given by Owen & Zienkiewicz (1957) and Elder (1959) for weakly shared, two-dimensional flow past wire grids. Unlike these earlier formulations, however, in the present study the equations of motion are solved without placing restrictions on the magnitude of variation of resistance across the grid. The resulting solution, taking account of streamline deflexions, is verified experimentally for moderately sheared flow past three grids constructed to produce three widely differing velocity distributions in a water tunnel of circular cross-section.

1. Introduction

The present study was undertaken to develop a method for producing prescribed longitudinal ship wake distributions in which model propellers could be tested in variable-pressure water tunnels. These wakes are, in general, of arbitrary distribution and departures from uniformity of flow are large. This paper is concerned with the development of a solution for describing such flows which are generated by non-uniform wire grids, and experimental confirmation of the solution. Three grids were constructed to produce velocity distributions which would check the theoretical results adequately and which were representative of wakes of interest in propeller testing. The wake producer grids were as follows:

Grid A. A grid constructed of horizontal cylindrical rods of variable spacing to produce a two-dimensional cosine resistance-coefficient distribution.

Grid B. A grid constructed of wire screens to produce a circumferentially varying cosine velocity distribution.

Grid C. A grid constructed of wire screens to produce the distribution of longitudinal flow velocity observed in the wake of a single-screw surface ship.

Published analytical work on steady flow past non-uniform wire grids has treated the two-dimensional problem. Owen & Zienkiewicz (1957) showed that for weakly sheared flows past wire grids located in a plane normal to the axis of a duct, a linear relationship exists between the downstream velocity distribution and the resistance-coefficient distribution across the grid. Two years later Elder (1959), using a more general approach, verified this solution and extended the formulation to cover the case of the screen of arbitrary shape. Both of these

formulations require that departures from uniformity of velocity and resistance coefficient be small, and are theoretically applicable only to weakly sheared flows. To test their solution, Owen & Zienkiewicz (1957) constructed a grid with a linear variation in resistance coefficient, and obtained surprisingly close agreement between the measured and computed velocity profiles for a value of shear parameter, τ, as high as 0·45. The measured downstream velocity profile was nearly linear and the slight non-linearity was partially ascribed to errors in the fabrication of the grid.

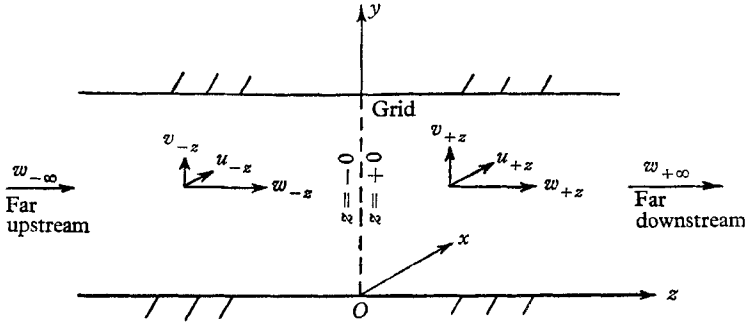

FIGURE 1. Co-ordinate system and grid arrangement.

In the present study the problem is extended to include three-dimensional flows and it is not required that departures in uniformity of velocity and resistance coefficient be small. It is hypothesized, however, that for moderately sheared flows streamline deflexions are sufficiently small to allow partial linearization of the equations of motion. A high-order solution of the partially linearized equations of motion is found which gives a non-linear relation between downstream velocity distribution and grid resistance-coefficient distribution. This solution appears to be in better agreement with the experimental results obtained by Owen & Zienkiewicz (1957), for a linear distribution of resistance coefficient, than is obtained from their first-order solution. For non-uniform flows where the effect of streamline deflexions is not negligible, an approximate method is developed for calculating streamline deflexion corrections to the resulting velocity distributions. The method is applied to GRID A and GRID C, and the numerical calculations for the corrections are summarized in table 4.

1.1. *Flow through a non-uniform wire grid*

On passing through a grid of non-uniform geometry, fluid is locally deflected and its static pressure is reduced (see figure 1). The discontinuity in lateral velocity due to the streamline deflexion may be described by a refraction coefficient, α, which expresses the ratio of the lateral velocity immediately downstream ($z = +0$) of the grid to that immediately upstream ($z = -0$) of the grid,

$$\alpha = \left(\frac{u_{+0}^2 + v_{+0}^2}{u_{-0}^2 + v_{-0}^2}\right)^{\frac{1}{2}}. \tag{1.1}$$

The pressure drop, Δp, across the grid may be described by a dimensionless resistance coefficient, K, which is based on the local velocity, w_0, normal to the grid,

$$K = (p_{-0} - p_{+0})/\tfrac{1}{2}\rho w_0^2. \tag{1.2}$$

Weighardt (1953) and other investigators have found that grid geometry and resistance coefficient may be related as follows:

$$K = cs/(1-s)^2, \tag{1.3}$$

where s is the solidity ratio of the grid, and c is a loss coefficient which is a function of Reynolds number, R_e. The characteristic Reynolds number, $w_0 d/(1-s)\nu$, is based on wire diameter and the interstitial velocity through the grid, $w_0/(1-s)$. For square-mesh wire screens Simmons & Cowdrey (1949) determined from experiment that for $300 < R_e < 400$ the loss coefficient, c, could be taken as approximately unity. Weighardt plotted the data obtained by Simmons & Cowdrey and other investigators, and obtained an empirical relation between R_e and c which fitted the experimental data very well for $60 < R_e < 600$. For $600 < R_e < 3000$ there was considerable scatter, most of the data indicating that $0{\cdot}65 < c < 0{\cdot}85$ in this range of Reynolds numbers. Cornell (1958) extended the plot of available data up to $R_e \approx 20{,}000$. For square-mesh wire screens he found that the loss coefficient levelled off to about 0·80 in the range $600 < R_e < 4000$, and then rose gradually to a value of 1·00 at $R_e \approx 15{,}000$. Cornell also plots data for flow normal to a bank of cylindrical tubes, where the loss coefficient remains approximately constant at about 0·70 for the range $2000 < R_e < 40{,}000$.

A conclusion that may be drawn from the above is that for either square-mesh wire screens or a bank of cylindrical tubes, for $10^3 < R_e < 10^4$, the loss coefficient remains relatively constant at a value somewhat less than unity. It was noted, however, that when Owen & Zienkiewicz (1957) produced a near-linear velocity profile downstream of a bank of cylindrical rods, the rod spacings were determined on the assumption that the loss coefficient could be taken as unity. A careful examination of the rod spacings adopted by Owen & Zienkiewicz indicated that the desired velocity distribution could not have been correctly calculated from their theoretical solution when using a loss coefficient of unity. Assuming that their theoretical solution is correct, and assuming that the loss coefficient, c, remained constant for the Reynolds number range covered in the experiment, $5000 < R_e < 9000$, it was found that c should be taken as 0·78. Available experimental data, as discussed above, indicates that such a value is not unreasonable, and it is used later for the design of Grid A, which is an arrangement of horizontal cylindrical rods.

Grid B and Grid C of this paper were constructed by arranging wire screens of various mesh sizes in carefully fitted patterns on a single support screen of low solidity ratio. All screens were of the square-mesh, plain-weave variety and made of stainless steel wire. The support screen used in every case was a 16×16 wires/in.^{2} mesh with a 0·009 in. wire diameter and a 0·267 solidity ratio. The resistance coefficient of each screen combination was determined from (1.2) based on measurements, made in a water tunnel, of pressure drop and flow velocity across the screens. The experimental results are shown in figure 2, along with an estimated resistance coefficient curve which was obtained by adding the individual resistance coefficients of the support and overlay screens as calculated from (1.3), taking $c = 0{\cdot}78$. For the Reynolds number range covered in the tests, $600 < R_e < 5000$, (based on the overlay screen geometry) the

change in combined resistance coefficient was found to be small. It was also found that changes in the orientation of the wires of one screen relative to the other had a negligible effect on resistance coefficient. The scatter of the experimental results in figure 2 can probably be attributed to departures of screen geometry from nominal dimensions, and dirt or scale which would occasionally collect on the screens. A list of the screens tested and measured resistance coefficients are given in table 1.

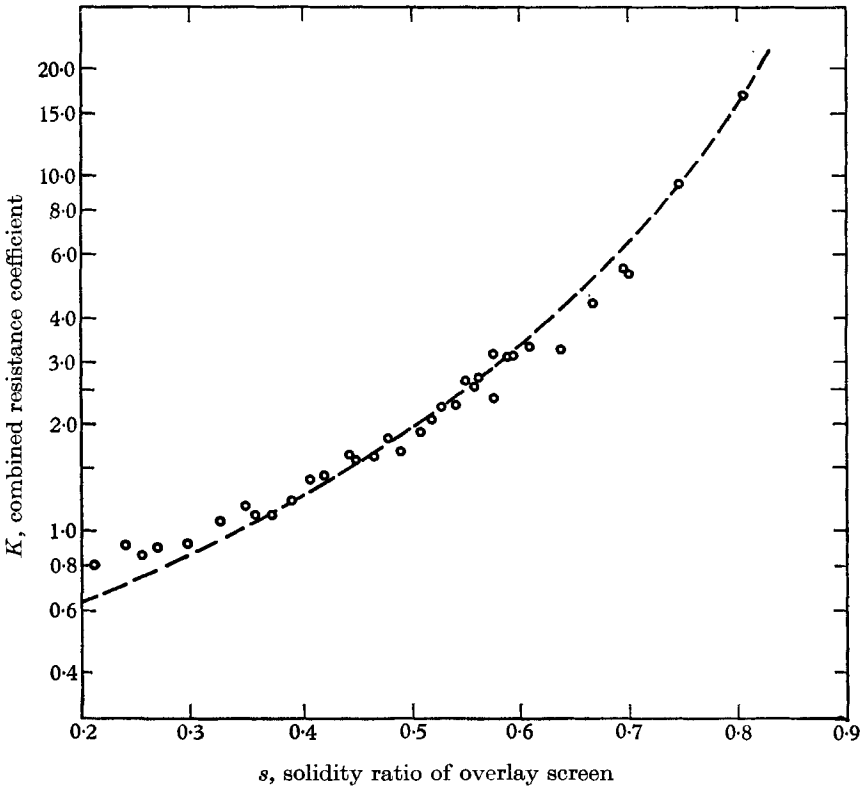

FIGURE 2. Plot of experimentally and theoretically determined relationship between K and s, for screens in combination with a 16 × 16 × 0·009 in. support screen.

In the present study the results of the experimental investigation of the refraction coefficient, α, made by Spangenburg (see Taylor & Batchelor 1949) will be assumed to hold for the three grids which were constructed to verify the solution which is later developed. From these tests, on the basis of lateral forces measured on square-mesh wire screens placed obliquely to the flow, it was found that the refraction coefficient, α, is independent of Reynolds number and empirically related to the resistance coefficient, K, by the expression

$$\alpha = b(1+K)^{-\frac{1}{2}} \quad (b = 1{\cdot}1). \tag{1.4}$$

While the experiments were confined to the Reynolds number range

$$80 < R_e < 300$$

it will be assumed here that this expression remains valid for higher Reynolds numbers, since the resistance coefficient itself, above this range, appears to be relatively insensitive to changes in Reynolds number. For the grids constructed of screens it will also be assumed, as was done by Taylor & Batchelor, that the refraction coefficient is '. . . rotationally symmetrical to its (the screen's) plane'.

	Overlay screen			
Number	Solidity ratio	Mesh	Wire diameter (in.)	Combined resistance coefficient
1†	0	—	—	0·42
2	0·211	4	0·0280	0·80
3	0·240	4	0·0320	0·90
4	0·254	8	0·0170	0·86
5	0·267	16	0·0090	0·89
6	0·296	18	0·0090	0·91
7	0·326	24	0·0075	1·07
8	0·350	26	0·0075	1·20
9	0·360	20	0·0100	1·10
10	0·373	12	0·0170	1·11
11	0·392	20	0·0110	1·22
12	0·407	10	0·0230	1·40
13	0·422	20	0·0120	1·41
14	0·444	32	0·0080	1·64
15	0·451	26	0·0100	1·61
16	0·466	18	0·0150	1·61
17	0·480	35	0·0080	1·87
18	0·492	18	0·0160	1·68
19	0·511	30	0·0100	1·90
20	0·517	18	0·0170	2·04
21	0·529	35	0·0090	2·24
22	0·542	24	0·0135	2·22
23	0·553	35	0·0095	2·64
24	0·558	24	0·0140	2·56
25	0·564	40	0·0085	2·70
26	0·577	10	0·0350	2·37
27	0·577	100	0·0035	3·17
28	0·590	40	0·0090	3·05
29	0·596	28	0·0130	3·06
30	0·609	50	0·0075	3·64
31	0·638	14	0·0280	3·20
32	0·668	12	0·0350	4·40
33	0·695	16	0·0280	5·48
34	0·702	14	0·0320	5·20
35	0·750	20	0·0250	9·45
36	0·806	20	0·0280	17·00

† Support screen, 16 × 16 × 0·0090 in. with no overlay screen.

TABLE 1. List of overlay screens and combined resistance coefficients.

2. The equations of motion

For steady incompressible flow past a wire grid of non-uniform properties it is assumed that viscosity effects are negligible except in the immediate vicinity of the grid. The plane of the grid, $z = 0$, is taken normal to the walls of an infinitely long duct of constant cross-section (see figure 1). Far upstream and far downstream of the grid the static pressure is taken to be uniform and the lateral velocity components are taken to be zero. It is found by experiment that upstream and downstream of a grid, these conditions are reached within a distance roughly equal to the lateral dimensions of the grid. At the grid, which is considered to be a surface of hydrodynamic discontinuity (see Batchelor 1945), the effect of fluid viscosity produces a static pressure drop across the grid and locally deflects streamlines. The problem is to find the relationship between the flow far upstream and far downstream of the grid and the resistance and refraction characteristics of the grid. In obtaining a linearized equation of motion, the principal assumption made is that streamline deflexions are small.

Neglecting body forces, we may write the equations of motion for the regions upstream or downstream of the grid as

$$\nabla H = \mathbf{q} \times \boldsymbol{\omega}, \tag{2.1}$$

where

$$\left.\begin{aligned} H &= p/\rho + \tfrac{1}{2}q^2, \quad \mathbf{q} \equiv (u, v, w), \\ \boldsymbol{\omega} &\equiv \nabla \times \mathbf{q} \equiv (\xi, \eta, \zeta). \end{aligned}\right\} \tag{2.2}$$

The velocity and vorticity components are taken in the respective directions of the co-ordinate axes (x, y, z). If the lateral velocity components, u and v, are everywhere small in comparison with the longitudinal velocity component, w, the streamlines in each region will be approximately parallel to the z co-ordinate axis. Neglecting viscosity, and assuming that streamline deflexions are sufficiently small, we may take vorticity to be constant along streamlines.† This assumption is consistent with the linearization procedure which will be followed in simplifying the equations of motion. The vorticity components may then be written in terms of the velocity components far upstream and far downstream of the grid, all changes in vorticity being confined to the plane of the grid, which is considered as a surface of hydrodynamic discontinuity. If we denote quantities in the upstream region and the downstream region by subscripts $-z$ and $+z$, respectively, and quantities far upstream and far downstream by $z = -\infty$ and $z = +\infty$, respectively, the vorticity is given by

$$\boldsymbol{\omega}_{\pm z} \simeq \boldsymbol{\omega}_{\pm\infty} = (\xi_{\pm\infty}, \eta_{\pm\infty}, \zeta_{\pm\infty}) = (\partial w_{\pm\infty}/\partial y, -\partial w_{\pm\infty}/\partial x, 0).$$

Substituting these expressions for the vorticity components into (2.1) we may write the equations of motion for either region as

$$\left.\begin{aligned} \partial H_{\pm z}/\partial x &= w_{\pm z}\partial w_{\pm\infty}/\partial x, \quad \partial H_{\pm z}/\partial y = w_{\pm z}\,\partial w_{\pm\infty}/\partial y, \\ \partial H_{\pm z}/\partial z &= -u_{\pm z}\,\partial w_{\pm\infty}/\partial x - v_{\pm z}\,\partial w_{\pm\infty}/\partial y. \end{aligned}\right\} \tag{2.3}$$

† For the case of two-dimensional flow, where $\boldsymbol{\omega} = (\xi, 0, 0)$, it may be shown from the Helmholtz equation that vorticity is necessarily constant along streamlines. For three-dimensional flow the assumed constancy of vorticity along streamlines is a reasonable approximation only for sufficiently small streamline deflexions.

Since streamline deflexions have been assumed small, and since by Bernoulli's equation the total head, H, in each region remains constant along streamlines,

$$\partial H_{\pm z}/\partial z \simeq 0,$$

and the equations of motion (2.3) reduce to

$$dH_{\pm z} = w_{\pm z} dw_{\pm \infty}.$$

To relate the flows in the regions upstream and downstream, this equation is evaluated in the immediate vicinity of the grid, $z = \pm 0$. Subtracting the resulting equations from one another, we find that

$$d(H_{-0} - H_{+0}) = w_0 d(w_{-\infty} - w_{+\infty}), \tag{2.4}$$

where, to satisfy continuity of flow normal to the grid,

$$w_{-0} = w_{+0} = w_0. \tag{2.5}$$

For small lateral velocity components, $q_{-0} \simeq q_{+0}$, and from (2.2) and (1.2),

$$H_{-0} - H_{+0} \simeq (p_{-0} - p_{+0})/\rho = \tfrac{1}{2} K w_0^2.$$

If we substitute this expression into (2.4), the equation of motion finally simplifies to

$$K dw_0 + \tfrac{1}{2} w_0 dK + d(w_{+\infty} - w_{-\infty}) = 0, \tag{2.6}$$

which is identical to the expression obtained by Elder (1959) for the case of two-dimensional flow. The equivalence between the two- and three-dimensional flows is a direct consequence of the assumption that streamline deflexions are small, which permits the same procedure for linearization of the equations of motion.

2.1. *The perturbation velocity potential*

In order to solve (2.6) it is necessary first to establish a relationship between w_0, $w_{+\infty}$ and $w_{-\infty}$. If the velocity components in the regions upstream and downstream of the grid are formulated in terms of perturbation velocities (indicated by *) which are superimposed on the basic flows at $z = \pm \infty$, then

$$u_{\pm z} = u^*_{\pm z}, \quad v_{\pm z} = v^*_{\pm z}, \quad w_{\pm z} = w^*_{\pm z} + w_{\pm \infty}. \tag{2.7}$$

Since, for the assumed case of small streamline deflexions, vorticity is taken constant along streamlines in the two regions of flow, the perturbation velocity field should not contribute vorticity to the basic flows which are given at $z = \pm \infty$. It follows, therefore, that the perturbation velocity field in each region may be uniquely described by a perturbation velocity potential which satisfies the Laplace equation, $\nabla^2 \Phi^* = 0$, where

$$u^*_{\pm z} = \partial \Phi^*_{\pm z}/\partial x, \quad v^*_{\pm z} = \partial \Phi^*_{\pm z}/\partial y, \quad w^*_{\pm z} = \partial \Phi^*_{\pm z}/\partial z. \tag{2.8}$$

For Cartesian co-ordinates a solution of the Laplace equation is possible assuming a separation of variables,

$$\Phi^* = X(x)\, Y(y)\, Z(z).$$

Evaluating only $Z(z)$, we can write the general solution (see, for example, Rouse 1959) as

$$\Phi^* = X(x)\,Y(y)\,(Ae^{lz}+Be^{-lz}).$$

From (2.7) it is obvious that the perturbation velocities must vanish at $z = \pm\infty$. Denoting the velocity potentials upstream and downstream of the grid by subscripts $-z$ and $+z$, respectively, one obtains

$$\Phi^*_{-z} = X(x)\,Y(y)\,A\,e^{lz}, \quad \Phi^*_{+z} = X(x)\,Y(y)\,B\,e^{-lz}. \tag{2.9}$$

Now the velocity at the grid, w_0, may be related to the velocities upstream and downstream, $w_{-\infty}$ and $w_{+\infty}$, by using the boundary conditions at the grid ($z = \pm 0$), as given by (1.1) and (2.5). To satisfy continuity of flow normal to the grid ($z = \pm 0$) substitution of (2.7), (2.8) and (2.9) into (2.5) yields the expressions

$$w_0 = w_{-\infty} + AX(x)\,Y(y), \quad w_0 = w_{+\infty} - BX(x)\,Y(y). \tag{2.10}$$

Equation (1.1), relating the lateral flow velocities on each side of the grid ($z = \pm 0$), upon substitution of (2.7), (2.8) and (2.9), yields the following expression for the constants A and B,

$$B = \alpha A. \tag{2.11}$$

Substitution of (2.11) into (2.10) leads to the equation

$$w_0 = \{1/(1+\alpha)\}(w_{+\infty} + \alpha w_{-\infty}). \tag{2.12}$$

It is of some interest to note that for the special case of continuity of lateral flow across the grid, $\alpha = 1$, which is the case in the 'actuator disk problem', the velocity at the grid, for a given streamline, is the average of those far upstream and far downstream of the grid. For the general case where lateral velocities are discontinuous across the grid, equation (2.12) holds.

2.2. *Solutions of the linearized equation of motion*

The desired differential equation of motion relating the resistance and refraction coefficients of the grid and the velocity components far upstream and far downstream may now be obtained by substituting (2.12) into (2.6). The derivation so far has been kept quite general in order to demonstrate that solutions which have been obtained previously by others follow from these same expressions. Two earlier solutions are given below, followed by the present solution.

(i) *Solution of Taylor & Batchelor* (1949). In this case departures of velocity from uniformity are small, and flow is past a grid of uniform properties. The velocities far upstream and far downstream may be written as

$$w_{-\infty} = 1 + \Delta w_{-\infty}, \quad w_{+\infty} = 1 + \Delta w_{+\infty}, \tag{2.13}$$

where $w_{-\infty}$ and $w_{+\infty}$ are made dimensionless by dividing through by the mean flow velocity past the grid. The resistance and refraction coefficients of the grid which are constant will be denoted by K_0 and α_0, respectively. Substitution of (2.13) and (2.12) into (2.6) yields

$$\frac{\Delta w_{+\infty}}{\Delta w_{-\infty}} = \frac{1+\alpha_0-\alpha_0 K_0}{1+\alpha_0+K_0}. \tag{2.14}$$

(ii) *Solution of Elder* (1959). If the resistance and refraction coefficients of the grid are not constant, but their departures from uniformity are small they may be expressed as follows:

$$\left.\begin{aligned} K &= K_0(1+\epsilon), \\ \alpha &= \frac{b}{(1+K)^{\frac{1}{2}}} = \alpha_0\left[1-\frac{1}{2}\frac{K_0}{1+K_0}\epsilon+\ldots\right], \end{aligned}\right\} \tag{2.15}$$

where

$$\alpha_0 = \frac{b}{(1+K_0)^{\frac{1}{2}}} \quad (\epsilon \ll 1).$$

Substitution of (2.13), (2.15) and (2.12) into (2.6) yields

$$K = K_0 + 2\left[\Delta w_{-\infty}\left(1-\frac{\alpha_0 K_0}{1+\alpha_0}\right) - \Delta w_{+\infty}\left(1+\frac{K_0}{1+\alpha_0}\right)\right], \tag{2.16}$$

where quantities of $O(\epsilon)^2$ and $O[(\Delta w_{\pm\infty})^2]$ are neglected.

(iii) *Present solution.* In the present solution departures of the resistance and refraction coefficients from uniformity will not be considered small, but the flow velocity far upstream of the grid, $w_{-\infty}$, will be taken as uniform. This assumption of uniform flow upstream of the grid corresponds to conditions normally existing in wind-tunnel and water-tunnel experiments. Substitution of (1.4) and (2.12) into (2.6) yields an equation of the form

$$dw/d\chi + wP(\chi) = Q(\chi), \tag{2.17}$$

where the following changes of variable have been made:

$$w = 1 - w_{+\infty}/w_{-\infty}, \quad \chi = (1+K)^{\frac{1}{2}};$$

the quantities $P(\chi)$ and $Q(\chi)$ are given by the expressions

$$P(\chi) = \frac{\chi^3+2b\chi^2-b}{(\chi+b)(\chi^3+b)}; \quad Q(\chi) = \frac{\chi(\chi+b)}{\chi^3+b}.$$

Equation (2.17) is a linear differential equation of the first order and has a solution of the form

$$w\exp\left[\int P(\chi)\,d\chi\right] = \int Q(\chi)\exp\left[\int P(\chi)\,d\chi\right]d\chi + C_1, \tag{2.18}$$

where C_1 is an arbitrary constant.

Evaluation of the integrals in (2.18) is made difficult by the presence of the constant b, appearing in the functions $P(\chi)$ and $Q(\chi)$, which arises from the empirical relation for the refraction coefficient given in (1.4). To simplify the solution, b is taken as unity and the functions are rewritten in the following form

$$P(\chi) = M(\chi^2+\chi-1)/(\chi^3+1), \quad Q(\chi) = N\chi(\chi+1)/(\chi^3+1).$$

A simple computation shows that for the range $0{\cdot}5 < K < 25$, M is within the range $0{\cdot}97 < M < 1{\cdot}01$, and N within the range $1{\cdot}01 < N < 1{\cdot}02$. As an approximation, then, M and N will be considered constants for a given grid. If M is taken as unity, it follows by direct integration that

$$\exp\left[\int P(\chi)\,d\chi\right] = \frac{(1+\chi^3)^{\frac{2}{3}}}{1+\chi}$$

and

$$\int Q(\chi)\exp\left[\int P(\chi)\,d\chi\right]d\chi = N(\chi+\tfrac{1}{6}\chi^{-2}-\tfrac{2}{45}\chi^{-5}\ldots).$$

Neglecting all but the first two terms in the series, the solution to (2.17) may be written finally as

$$w' = 1 - \frac{1+\chi}{(1+\chi^3)^{\frac{2}{3}}} N\left[\frac{\frac{1}{6}+\chi^3}{\chi^2} - \gamma_0\right], \tag{2.19}$$

where $\chi = (1+K)^{\frac{1}{2}}$, $w' = 1-w$, and $\gamma_0 = -C_1/N$. The unknown constant γ_0 may be determined by integrating each side of (2.19) over the cross-sectional area, A, of the duct. Noting that for continuity of flow,

$$\int_A (1-w')\,dA = 0,$$

it follows that

$$\gamma_0 = \int_A \frac{1+\chi}{(1+\chi^3)^{\frac{2}{3}}} \frac{\frac{1}{6}+\chi^3}{\chi^2}\,dA \Big/ \int_A \frac{1+\chi}{(1+\chi^3)^{\frac{2}{3}}}\,dA.$$

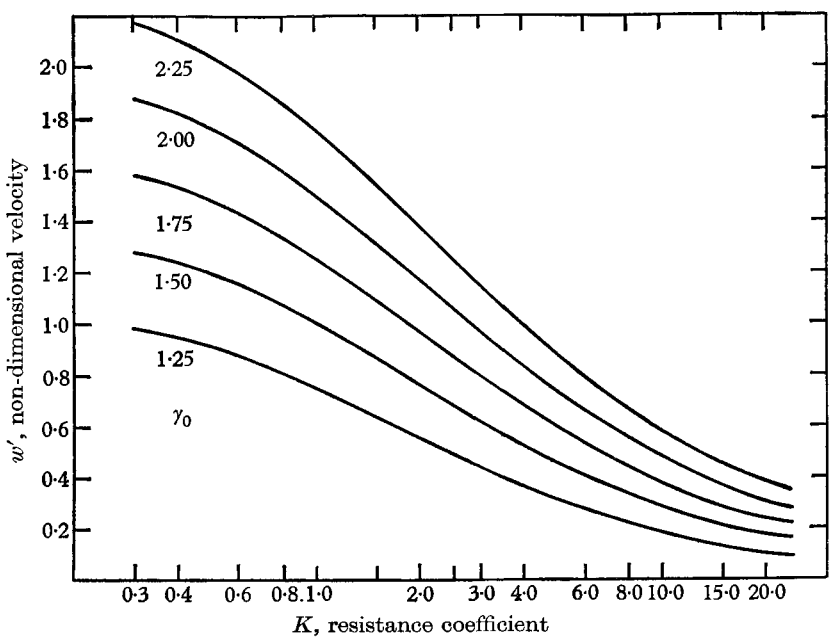

FIGURE 3. Plot of equation (2.19), giving relationship between K and w' for a range of γ_0.

Equation (2.19) is plotted in figure 3 for a range of γ_0-values, taking $N = 1{\cdot}02$. For the design of a given grid, γ_0 would be determined by selecting a screen having minimum K to produce the highest velocity desired. Substitution of $w'_{\max}$ and $K_{\min}$ into (2.19) would then allow γ_0 to be determined. To complete the design of the grid for a prescribed distribution of velocity, w', the distribution of K could then be determined graphically from figure 3 or from a replot of equation (2.19) for the particular γ_0 which is adopted.

In figure 4 the two-dimensional velocity distributions downstream of three grids having linear variations in resistance coefficient have been calculated according to (2.19) and the first-order solution given by (2.16). The case considered is for uniform flow far upstream of grids which are placed in a duct of

rectangular cross-section ($0 \leqslant y \leqslant h$). For each grid $K_{\min} = 0{\cdot}5$. For comparison purposes the downstream velocity distributions are characterized by a shear parameter, τ, which is defined as

$$\tau = |\partial w'/\partial y'|, \quad y' = y/h.$$

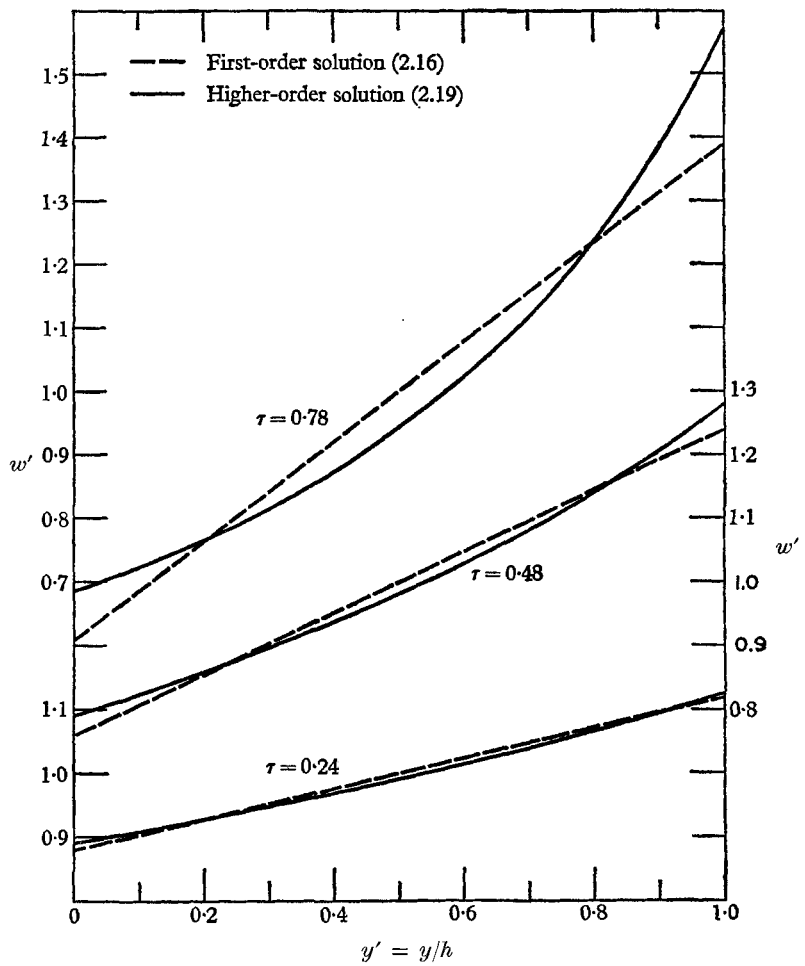

FIGURE 4. Comparison of theoretical velocity distributions for grids having linear resistance distributions.

In table 2 the percentage differences, based on mean flow velocity, between velocities given by (2.16) and (2.19) are given for the three grids. The first-order solution is theoretically applicable only to weakly sheared flows, where departures from uniformity of velocity and resistance coefficient are small, and it is seen that for $\tau > 0{\cdot}50$ the differences in resulting velocity distribution will exceed 4 %. The higher-order solution, applicable to moderately sheared flows, will presumably also break down at some higher value of τ where the assumed constancy of vorticity along streamlines is no longer valid. This upper limit needs to be determined by experiment.

The non-linear relation between velocity and resistance coefficient given by (2.19) is borne out by the experimental data obtained by Owen & Zienkiewicz (1959) for a grid with a linear distribution of resistance coefficient. These data are reproduced in figure 5 along with theoretical predictions given by (2.16) and (2.19), taking $C = 0{\cdot}78$ as was discussed in the Introduction. The agreement is better when using (2.19), but for this case, where $\tau = 0{\cdot}45$, the differences between the first-order and higher-order solutions is not appreciable.

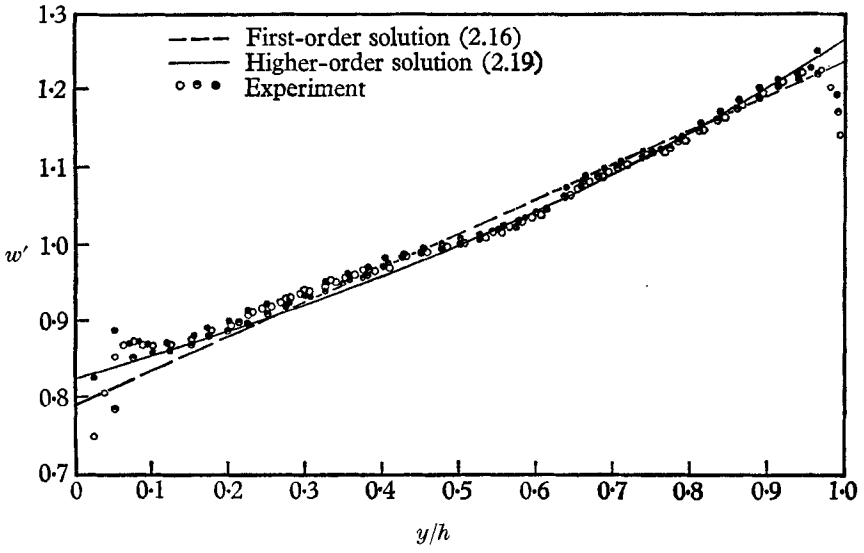

FIGURE 5. Comparison of theoretical and experimental velocity distributions, from measurements by Owen & Zienkiewicz (1957).

	$\Delta w'$ (%)		
τ	$y' = 0$	$y' = 0{\cdot}5$	$y' = 1{\cdot}0$
0·24	−1	1	−1
0·48	−3	2	−4
0·78	−8	6	−18

TABLE 2. Percentage differences for velocity distributions of figure 4.

3. The effect of streamline deflexions

In the derivation of (2.19) linearization of the equations of motion has been made possible by assuming that streamline deflexions downstream of the grid are small. This assumption has allowed the streamlines to be replaced by straight lines parallel to the walls of the duct, along which both vorticity, ω, and total head, H, have been taken as constant. The solution given by equation (2.19), then, applies along straight streamlines, where the local velocity far downstream of the grid at a point in the lateral (x, y)-plane is produced by the local resistance coefficient at a point having the same lateral co-ordinates in the plane of the grid. For flow past a grid of non-uniform properties this condition will be

approached when $w_0 \to w_{+\infty}$, which occurs as $w_{+\infty}/w_{-\infty} \to 1$, or as $K \to \infty$ (see equation (2.12)). The first limiting case, $w_{+\infty}/w_{-\infty} \to 1$, is not of particular interest here since it corresponds to weakly sheared flows. The second limiting case, $K \to \infty$, is not of practical interest since it will usually be necessary to use grids with low mean resistance-coefficients in order to obtain high flow velocities in test facilities which have limited power supplies. The following considerations are relevant therefore, for cases of moderately sheared flows where it is necessary to estimate the effect of streamline deflexions on the resulting velocity distributions.

A grid may be represented by a number of elementary areas, $A_i(0)$, each element being associated with some average local resistance coefficient, K_i, and some average local longitudinal velocity, $w_i(0)$. These elements make up the cross-sectional areas of a collection of stream tubes which extend from the plane of the grid to far downstream. The manner in which $A_i(z)$ varies along a given stream tube is governed by the requirements that the flow rate be constant along each stream tube, that the sum of flow rates through all stream tubes at each cross-section of the duct be constant and equal to the total flow rate, and that the sum of the cross-sectional areas of the stream tubes be constant and equal to the duct cross-sectional area. These conditions may be summarized as

$$w_i(z)\, A_i(z) = \text{const.} = Q_i, \tag{3.1}$$

$$\sum_{i=1}^{N} w_i(z)\, A_i(z) = \text{const.} = Q, \tag{3.2}$$

$$\sum_{i=1}^{N} A_i(z) = \text{const.} = A, \tag{3.3}$$

where N is the total number of grid elements considered. If $w_i(z)$ is non-dimensionalized on the mean flow velocity, $Q = A$.

Because streamline deflexions have not been taken into account in the solution given by (2.19) the above conditions will not necessarily be satisfied. To correct this deficiency the calculated velocity distribution will be adjusted according to the following approximate method. Two cases will be considered. (i) For a given K_i and corresponding $A_i(0)$ distribution, find the corrected velocity distribution far downstream, $w_i(+\infty)$, and its corresponding area distribution, $A_i(+\infty)$. (ii) For a given velocity far downstream, $w_i(+\infty)$, and corresponding $A_i(+\infty)$ distribution, find the corrected resistance coefficient distribution, K_i, and its corresponding area distribution, $A_i(0)$. Case (i), which is simplest, will be considered first, and the corrections for case (ii) will follow.

For a given K_i and $A_i(0)$ distribution, the first estimate of $w_i(+\infty)$ is given by (2.19) and $w_i(0)$ by (2.12). If (3.1) is evaluated at the grid ($z = 0$) and far downstream ($z = +\infty$), a first estimate of $A_i(+\infty)$ will be given by

$$A_i(+\infty) = Q_i(0)/w_i(+\infty),$$

where

$$Q_i(0) = w_i(0)\, A_i(0).$$

But, in general,

$$\sum_{i=1}^{N} A_i(+\infty) \neq A,$$

which is contrary to the requirement set forth in (3.3). To satisfy (3.3) the corrected distribution of $A_i(+\infty)$, denoted $A_i(+\infty)^*$, will be approximated by

$$A_i(+\infty)^* = \frac{A}{\sum_{i=1}^{N} A_i(+\infty)} A_i(+\infty) \tag{3.4}$$

Rod	$\lvert y\rvert$ (in.)	Rod	$\lvert y\rvert$ (in.)	Rod	$\lvert y\rvert$ (in.)
1	0·106	9	1·837	17	3·813
2	0·318	10	2·063	18	4·108
3	0·531	11	2·293	19	4·426
4	0·745	12	2·527	20	4·773
5	0·960	13	2·767	21	4·158
6	1·176	14	3·013	22	5·589
7	1·394	15	3·268	—	—
8	1·614	16	3·534	—	—

TABLE 3. Calculated rod spacings for GRID A.

Noting that, in general, $\sum_{i=1}^{N} Q_i(0) \neq Q$, the corrected distribution of $Q_i(0)$, denoted $Q_i(0)^*$, will be approximated by

$$Q_i(0)^* = \frac{Q}{\sum_{i=1}^{N} Q_i(0)} Q_i(0),$$

and the final corrected distribution of $w_i(+\infty)$, denoted $w_i(+\infty)^*$, is then given by

$$w_i(+\infty)^* = \frac{Q_i(0)^*}{A_i(+\infty)^*}. \tag{3.5}$$

The calculation of $A_i(+\infty)^*$ and $w_i(+\infty)^*$ has been made for GRID A and GRID C of this paper and the numerical procedure is given in table 4.

For case (ii), where it is desired to find K_i and its corresponding $A_i(0)$ distribution for a given $w_i(+\infty)$ and $A_i(+\infty)$ distribution, the same procedure is followed initially to determine $w(+\infty)^*$ and $A_i(+\infty)^*$. $A_i(0)$ is then modified by the ratio $A_i(+\infty)/A_i(+\infty)^*$ and the K_i distribution calculated by (2.19) for a w' modified by the ratio $w_i(+\infty)/w_i(+\infty)^*$. This procedure is repeated until the desired $A_i(+\infty)$ and $w_i(+\infty)$ distributions are obtained.

4. Experimental results

To verify the solution, experiments were performed in the 12 in. water tunnel at the Hydromechanics Laboratory, David Taylor Model Basin. The tunnel, which has an open-jet test section, was modified as shown in figure 6. A Lucite duct made in two halves was inserted in the test section, and extended downstream of the entrance nozzle for a distance of 37 in. Each grid tested was mounted between mating flanges on the two halves of the duct and the entire duct assembly was held rigidly in place by four long bolts, threaded into the collector flange, which could be screwed tightly against the duct flange. The two halves of the

duct were kept in alignment by dowel pins which joined the matching flanges together. Velocity surveys in the duct were made using a rake of 0·125 in. diameter static and impact tubes, attached to a hollow shaft which could be rotated about and translated along the axis of the duct. Without the grids, at

GRID A

i	$\lvert y/a\rvert$	K_i	$w_i(+\infty)$	$w_i(0)$	$A_i(0)$	$Q_i(0)$	$A_i(+\infty)$	$A_i(+\infty)$*	$w_i(+\infty)$*
1	0	2·73	0·78	0·86	0·50	0·43	0·55	0·55	0·80
2	0·1	2·67	0·79	0·87	0·99	0·85	1·08	1·07	0·81
3	0·2	2·51	0·82	0·89	0·98	0·87	1·06	1·05	0·83
4	0·3	2·25	0·86	0·91	0·95	0·87	1·01	1·00	0·88
5	0·4	1·92	0·93	0·96	0·92	0·88	0·95	0·94	0·94
6	0·5	1·56	1·02	1·01	0·87	0·87	0·86	0·86	1·03
7	0·6	1·20	1·12	1·07	0·80	0·86	0·77	0·76	1·13
8	0·7	0·87	1·23	1·13	0·71	0·81	0·65	0·65	1·25
9	0·8	0·61	1·34	1·18	0·60	0·71	0·53	0·53	1·36
10	0·9	0·45	1·42	1·22	0·44	0·53	0·38	0·37	1·44
11	1·0	0·39	1·44	1·23	0·10	0·12	0·09	0·08	1·48
					7·86	7·80	7·91		

GRID C

i	K_i	$w_i(+\infty)$	$w_i(0)$	$A_i(0)$	$Q_i(0)$	$A_i(+\infty)$	$A_i(+\infty)$*	$w_i(+\infty)$*
1	0·42	1·23	1·12	32·09	35·90	29·20	28·10	1·31
2	1·07	0·99	0·99	5·19	5·16	5·22	5·02	1·05
3	1·41	0·90	0·94	4·39	4·13	4·59	4·41	0·96
4	2·04	0·77	0·86	4·03	3·47	4·51	4·35	0·82
5	3·05	0·63	0·76	3·18	2·42	3·84	3·69	0·67
6	5·20	0·46	0·63	5·08	3·18	6·91	6·64	0·49
7	17·00	0·20	0·36	2·45	0·88	4·40	4·23	0·21
				56·41	55·14	58·67		

TABLE 4. Summary of calculations of the corrected velocity and area distributions far downstream of GRID A and GRID C. The method of calculation is presented in § 3.

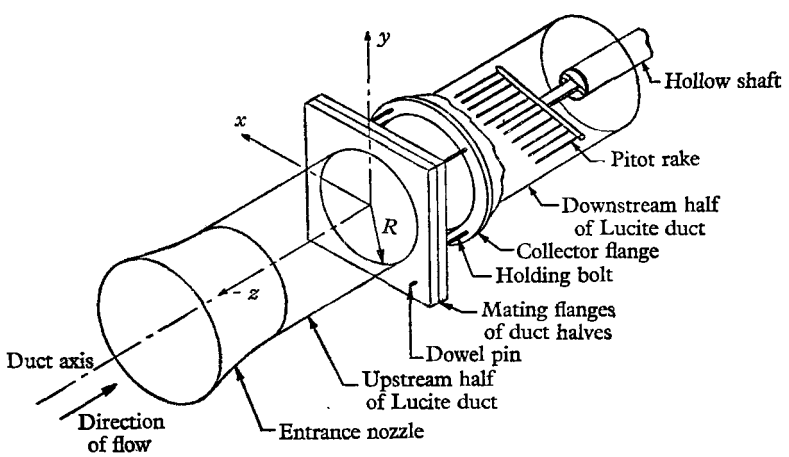

FIGURE 6. Duct arrangement for experiments in David Taylor Model Basin 12-in. water tunnel.

a section located 2 in. upstream of the interface between the connecting halves of the duct, for water speeds of 6 and 11 ft./sec the respective velocity variations were less than $\pm 2\,\%$ and $\pm 1\frac{1}{2}\,\%$. In both cases the velocity increased radially outwards from the centre-line of the duct. The boundary layer was approximately $\frac{1}{2}$ in. thick.

The three grids which were tested to verify the solution (2.19) are discussed in the following sections. For GRID A and GRID C the effect of streamline deflexions has been calculated.

4.1. *GRID A*

GRID A was constructed of parallel cylindrical rods to give a cosine resistance coefficient distribution in the y-direction (see figure 6). The rod spacing (ξ) was determined according to (1.3), taking $c = 0{\cdot}78$, such that

$$\frac{K}{c} = \frac{d/\xi}{(1-d/\xi)^2} = 2 + \tfrac{3}{2}\cos\left[|y/R|\,\pi\right].$$

The rods were made from stainless-steel precision shafting having a diameter, d, of 0·1247 in. (+0·0000 in., −0·0002 in.), and the calculated locations of the rods are given in table 3. The measured rod spacings varied less than $\pm 1\,\%$ from the calculated values.

The first tests made on the grid indicated that at mean water speeds greater than about 1 ft./sec the rods near the axis of the duct began to vibrate due to vortex shedding. At speeds of about 2 ft./sec vibrations of the rods was of such a high amplitude that flow near the axis, downstream of the rods, was nearly completely choked off. In an effort to increase the speed at which vibration began, a $\frac{1}{16}$ in. thick faired strut was inserted to restrain the rods along their mid-span. The measured velocity decrement downstream and directly behind the strut was approximately 2 %. With the centre support strut inserted it was found that vibration did not occur up to a mean water speed of about 5 ft./sec.

Velocity measurements were taken one duct diameter (12 in.) downstream of the rods, with centre support strut, at a mean water speed of 4·2 ft./sec. Non-dimensionalized values of the velocities recorded are shown in figure 7. At distances from 12 to 20 in. downstream of the grid the pressure was constant over the duct cross-section and no significant change was measured in the velocity distribution. (The relatively short length of the duct prevented making surveys further downstream.) Each experimental point plotted in figure 7 represents the average of velocities measured at corresponding locations in the four quadrants of the circular duct. The measured variations at corresponding locations were less than $\pm 3\,\%$, and are attributed primarily to the unsteady nature of the flow, which caused the water levels in the manometers to fluctuate while each reading was taken.

Figure 7 also shows the calculated velocity distributions according to the first-order solution (2.16), the higher-order solution (2.19), and the higher-order solution with corrections for the effect of streamline deflexions. The calculations for the corrected distribution are given in table 4, and it is noted that the corrections are quite small for this particular grid. While the corrected

distribution appears to be in best agreement with the experimental points the maximum deviation is about 3 %), the first-order solution gives fair agreement, the greatest differences occurring in the regions $|y/R| < 0{\cdot}2$ and $|y/R| > 0{\cdot}8$. These differences are roughly as would be expected based on the previous comparisons shown in figure 4 and figure 5.

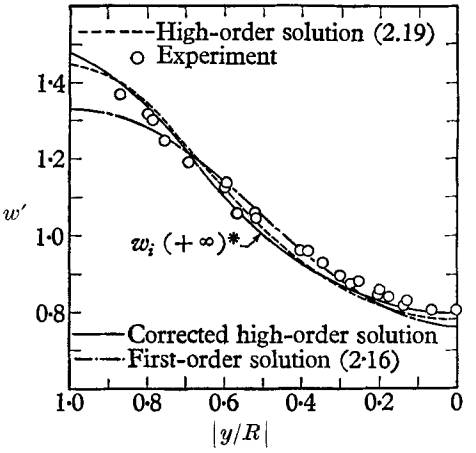

FIGURE 7. Comparison of theoretical and experimental velocity distributions for GRID A.

4.2. *GRID B and GRID C*

These grids were constructed by arranging square-mesh wire screens of varying mesh sizes in specified patterns on a support screen of 16×16 wires/in^2. with an 0·009 in. wire diameter and a 0·267 solidity ratio. The resistance coefficients of the various screen combinations were determined experimentally (see table 1) and it has been assumed that the refraction coefficients calculated by (1.4), using the combined resistance coefficients, are valid for a double layer of screens.

The fabrication of the grids required great care in order to piece them together accurately. After trying a number of rather crude schemes, which proved unsatisfactory, the following method of fabrication was finally adopted in assembling GRID B and GRID C:

(1) The required screen pattern was drawn on a $\frac{1}{8}$ in. thick aluminium sheet and the pieces were cut out using a $\frac{1}{64}$ in. thick band-saw blade. A number of $\frac{1}{8}$-in. diameter holes were then drilled in each pattern.

(2) The required overlay screens were glued to the patterns and cut to size using the band saw.

(3) The support screen was stretched and soldered to a stainless-steel frame; the aluminium-plus-screen patterns were laid out on the support screen, and through each hole the overlay and support screen wires were then spot welded together.

(4) Solvent was applied to the glue and the aluminium patterns were removed. Final welding of the screens was then completed.

GRID B was designed according to equation (2.19) to produce a circumferentially varying sinusoidal velocity distribution as given by the formula

$$w' = 1 + \tfrac{1}{2}(r/R)^2 \sin 2\theta,$$

where r/R is the non-dimensional radius. Since the velocity distribution for this grid is similar to that for GRID A, where streamline deflexion corrections were found to be small, no corrections have been calculated for this grid. The distribution of grid resistance required to produce the desired velocity distribution according to the high-order solution (2.19), along with the actual screens selected and their measured resistance coefficients are shown in figure 8. It will be noted that in certain instances the screens used depart somewhat from the

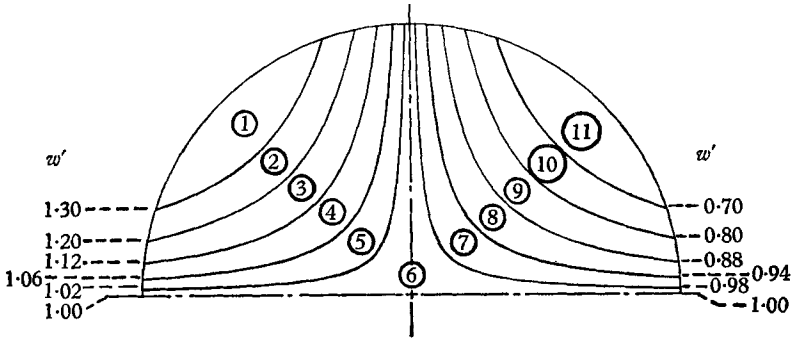

FIGURE 8. Outline drawing of upper half of GRID B showing lines of constant velocity and overlay screen arrangement, according to high-order solution (2.19).

Area	Overlay screen geometry	Actual K	Required K
1	None	0·42	0·42
2	$4 \times 4 \times 0{\cdot}028$	0·80	0·65
3	$8 \times 8 \times 0{\cdot}017$	0·86	0·88
4	$20 \times 20 \times 0{\cdot}010$	1·10	1·10
5	$20 \times 20 \times 0{\cdot}011$	1·22	1·25
6	$20 \times 20 \times 0{\cdot}012$	1·41	1·40
7	$18 \times 18 \times 0{\cdot}015$	1·61	1·55
8	$18 \times 18 \times 0{\cdot}016$	1·68	1·70
9	$18 \times 18 \times 0{\cdot}017$	2·04	2·10
10	$35 \times 35 \times 0{\cdot}0095$	2·64	2·60
11	$14 \times 14 \times 0{\cdot}028$	3·20	3·40

required resistance coefficients; this is due to the limited number of screens available for grid fabrication. The measured and calculated velocity distributions are shown in figure 9. The measurements were taken one duct diameter downstream of the grid ($z/R = 2{\cdot}0$) where the static pressure was found to be uniform. No significant change was measured in the velocity distribution at $z/R = 3{\cdot}0$, the furthest position downstream of the grid investigated. The maximum deviation of theory from experiment amounts to about 3% of the mean velocity. It may be concluded that the method of grid fabrication adopted is quite satisfactory and that a relatively small number of area elements may be used to produce a given velocity distribution. The latter point is important in reducing the time spent in fabricating grids.

GRID C was designed to produce the axial velocity distribution in the wake of a 'typical' single-crew surface ship. Rather than simulate a given ship wake, a distribution of resistance coefficient using available screens was chosen which

would produce a fictitious but typically severe ship wake and which would permit checking of the high-order solution taking streamline deflexions into account. The arrangement of the screens for this grid is shown in figure 10. Also shown is the calculated area and corresponding velocity distribution far

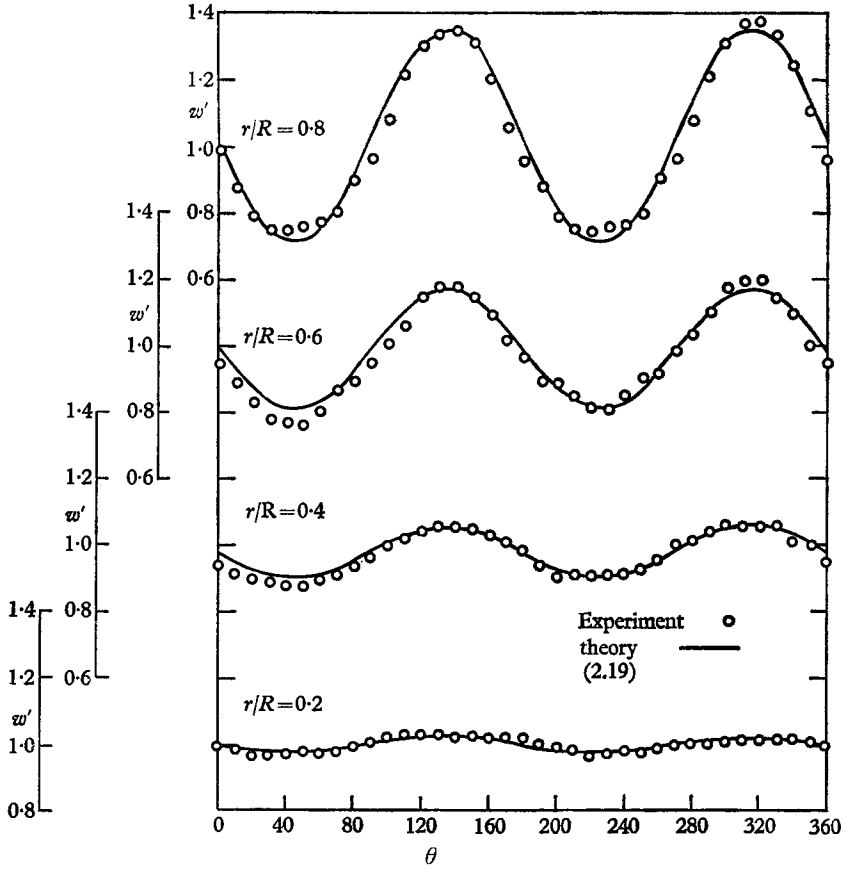

FIGURE 9. Measured and calculated velocities for grid designed to produce a sinusoidal velocity distribution (GRID B).

downstream, according to the high-order solution (2.19), taking streamline deflexions into account. The calculated corrections are appreciable and a summary of their computation is given in table 4. In applying the area corrections the points of intersection of the demarcation lines with the vertical centre-line have been assumed to remain fixed. Except in the regions close to these points the area corrections have been applied uniformly along the lines of demarcation of the area elements in the plane of the grid by displacing these lines in a direction normal to themselves.

The measured and calculated velocity distributions, according to the high-order solution (2.19) taking into account streamline deflexion corrections, are shown in figure 11. The corrected theoretical curve is shown as a stepwise distribution of velocity in order to accentuate the stepwise nature of the re-

sistance distribution of the screens. The measured velocities are given for three axial positions downstream of the grid, $z/R = 0{\cdot}5$, $2{\cdot}0$ and $3{\cdot}0$. The measurements revealed that static pressure did not become uniform until a position nearly one duct diameter downstream of the grid, $z/R = 2{\cdot}0$. Further downstream of

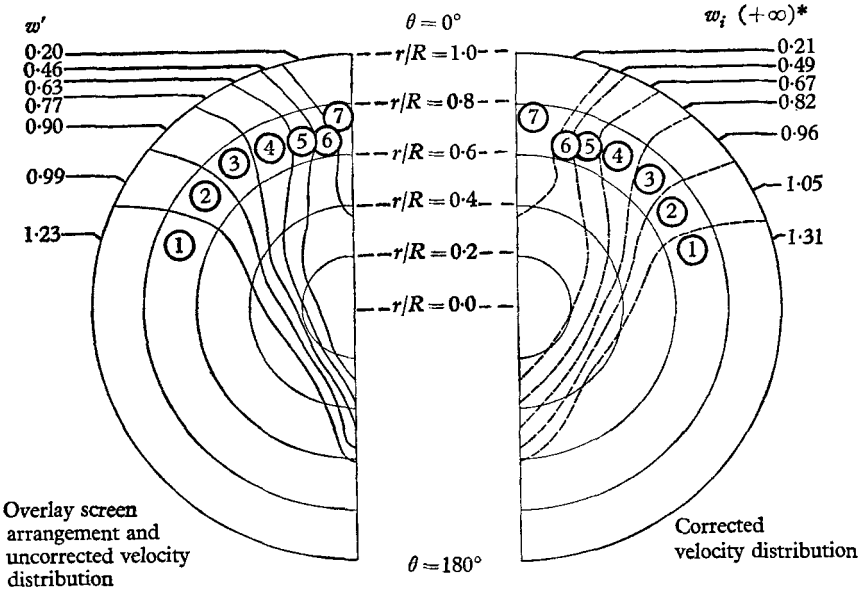

FIGURE 10. Outline drawing of GRID C showing overlay screen arrangement and uncorrected and corrected velocity distributions, according to high-order solution (2.19).

Area	Overlay screen geometry	Actual K
1	None	0·42
2	24 × 24 × 0·0075	1·07
3	20 × 20 × 0·012	1·41
4	18 × 18 × 0·017	2·04
5	40 × 40 × 0·009	3·05
6	14 × 14 × 0·032	5·20
7	20 × 20 × 0·028	17·00

Area element ...	1	2	3	4	5	6	7
First-order solution (2.16)	1·35	1·20	1·13	0·98	0·75	0·27	−2·40
High-order solution (2.19) *with streamline deflexion corrections*	1·31	1·05	0·96	0·82	0·67	0·49	0·21

TABLE 5

this position the experimental results indicate that in areas of large velocity gradient the axial velocities tended to equalize. As would be expected, then, the calculated and measured velocities are in best agreement for the $z/R = 2{\cdot}0$ position (indicated by a dashed line in figure 11) where the static pressure has

become uniform and where decay of the high velocity gradients has not yet begun.

For comparison the velocity distribution has been calculated according to the first-order solution (2.16). As can be seen in table 5 these velocities are in poor

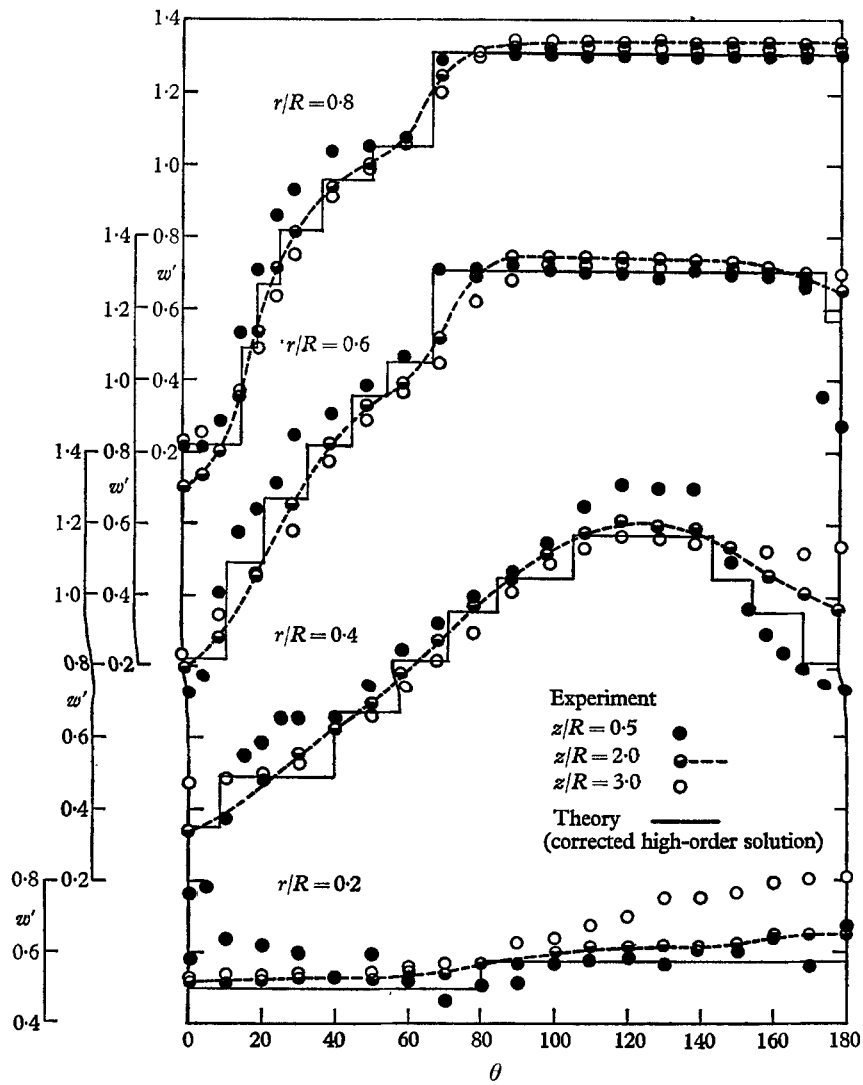

FIGURE 11. Measured and calculated velocities for the grid designed to produce the axial velocity distribution in the wake of a single-screw surface ship (GRID C).

agreement with those calculated using the high-order solution (2.19) with streamline deflexion corrections. It is concluded that the present solution is adequate for designing grids to produce moderately sheared flows of severity comparable to that produced by GRID C. The particular method of grid fabrication employed appears to be satisfactory.

This work was carried out at the Hydromechanics Laboratory of David Taylor Model Basin and is published by permission of its Director. Special thanks are given to Mr Angelo Campo who assisted in performing the experimental portion of this study, and to members of the shop who perfected the method of fabricating grids from wire screens.

REFERENCES

BATCHELOR, G. K. 1945 On the concept and properties of the idealized hydrodynamic resistance. *Aust. Counc. Aero. Rep. A.C.A.* 13.

CORNELL, W. G. 1958 Losses in flow normal to plane screens. *Trans. ASME*, **80**, 791–99.

ELDER, J. W. 1959 Steady flow through non-uniform gauzes of arbitrary shape. *J. Fluid Mech.* **5**, 355–68.

OWEN, P. R. & ZIENKIEWICZ, H. K. 1957 The production of uniform shear flow in a wind tunnel. *J. Fluid Mech.* **2**, 521–31.

ROUSE, H. 1959 *Advanced Mechanics of Fluids.* New York: Wiley and Sons.

SIMMONS, L. F. G. & COWDREY, C. F. 1949 Measurements of the aerodynamic forces acting on porous screens. *Aero. Res. Counc. R & M* 2276.

TAYLOR, G. I. & BATCHELOR, G. K. 1949 The effect of wire gauze on small disturbances in a uniform stream. *Quart. J. Mech. Appl. Math.* **2**, 1–29.

WEIGHARDT, K. E. G. 1953 On the resistance of screens. *Aero. Quart.* **4**, 186–92.